Aust. J. Phys., 1974, **27**, 597–627

A 1667 MHz OH Absorption Survey of the Southern Milky Way

J. L. Caswell and B. J. Robinson

Division of Radiophysics, CSIRO, P.O. Box 76, Epping, N.S.W. 2121.

Abstract

A search has been made at 1667 MHz for OH absorption against 105 strong continuum sources in the region $265° < l < 352°$, and data are presented for 33 sources showing absorption. The overall distribution of OH absorption in this galactic longitude range has been investigated by combining these results with measurements on 11 additional sources studied in earlier searches. Many of the sources showing 1667 MHz absorption have been observed at the other three 18 cm OH transitions and as a result 14 new satellite-line emission sources have been found.

1. Introduction

Robinson *et al.* (1971) and, in more detail, Robinson *et al.* (1974, present issue pp. 575–96; hereinafter referred to as Paper 1) have reported the results of a 1665 MHz search for OH in the southern Milky Way, designed primarily to detect new emission sources which are generally more intense at 1665 MHz than at 1667 MHz. The present paper reports the results of a complementary search of 105 strong continuum sources for OH absorption on the 1667 MHz transition. A secondary objective was to search for emission more intense at 1667 than at 1665 MHz, but none was found.

2. Observations

The instrumentation and observing technique were as used in the 1665 MHz search and as described more fully by Robinson *et al.* (1970). Briefly, the Parkes 64 m radio telescope was employed with the 10 kHz bandwidth filters of the 64-channel spectrometer. The continuum sources observed were selected from the Parkes 2700 MHz galactic survey and the velocity range of the search was ~ 100 km s^{-1} centred on the radial velocities of HII regions at nearby galactic longitudes. Integration times of 8 min on source resulted in peak-to-peak noise levels of $\sim 1{\cdot}3$ K. The telescope beamwidth to half-power was $12'{\cdot}2$ arc at 1667 MHz. The ratio of flux density to antenna temperature was $1{\cdot}59 \times 10^{-26}$ W m^{-2} Hz^{-1} K^{-1} for an unpolarized point source, based on an assumed flux density of 36×10^{-26} f.u.* for the source Hydra A.

A feed accepting linearly polarized radiation with the *E*-plane vertical was used during the search. For 30 of the 33 sources showing 1667 MHz absorption additional observations with both senses of circular polarization were made in several periods between May 1970 and April 1971. Twenty-two of the sources were also observed at 1665 MHz, 18 of them at 1612 MHz and 14 at 1720 MHz.

* 1 flux unit (f.u.) = 10^{-26} W m^{-2} Hz^{-1}.

Table 1. OH absorption in the longitude range 265°–352°

(1) Continuum source number	(2) Position (1950) R.A. h m s	(3) Dec. ° ′	(4)	(5)	(6)	(7)	(8)	(9)	(10)	(11)	(12)	(13)	(14)	(15)
					OH absorption			Continuum temperature						
			V_{lsr} (km s^{-1})	T_{1612} (K)	T_{1665} (K)	T_{1667} (K)	T_{1720} (K)	T_g (K)	T_s (K)	T_c (K)	T_{1667}/T_c	τ_{1667}	Fig.	Refs[A]
G265·1+1·5	08 57 34	−43 32·2	+6		1·2	2·3	1·0	1	15	15·5	0·148	0·161		M
G267·9−1·1	08 57 14	−47 19·7	+2	1·1	9·6	14·8	4·9	2	93	94	0·157	0·171		M
G274·0−1·1	09 22 49	−51 46·7	+37		0·6	1·1		0	20·5	20·5	0·054	0·056	1	
G282·0−1·2	10 04 55	−56 56·4	−5		0·75	1·2		4	19	21	0·057	0·059		M
G282·0−1·2	10 04 55	−56 56·4	−9	0·5		—		4	19	21	—	—		M
G284·3−0·3	10 22 27	−57 31·1	−13			1·5		4	112	114	0·013	0·013		M
G284·3−0·3	10 22 27	−57 31·1	0			0·6		4	112	114	0·005	0·005		M
G287·5−0·6	10 42 12	−59 22·6	−25		1·2	1·2		4	94	96	0·013	0·013		M
G291·3−0·7	11 09 50	−61 01·7	−26	2·1	6·6	7·9	1·2	2	47	48	0·165	0·181		M
G291·6−0·5	11 13 15	−60 58·5	−12	1·1	1·5	1·3		2	108	109	0·012	0·012		M
G298·9−0·4	12 12 42	−62 44·0	+19		0·6	2·1		4	26	28	0·075	0·078	2	R
G298·9−0·4	12 12 42	−62 44·0	+26		0·5	0·7		4	26	28	0·025	0·025	2	R
G305·2+0·0	13 08 09	−62 29·0	−46			1·2		4	25	27	0·044	0·045	3	
G305·2+0·0	13 08 09	−62 29·0	−33			1·0		4	25	27	0·037	0·038	3	
G305·4+0·2	13 08 43	−62 19·6	−40			1·9		4	48	50	0·038	0·039		G
G311·6+0·3	14 01 17	−61 05·5	−55			1·2		6	7	10	0·120	0·128		G
G311·9+0·1	14 04 03	−61 11·0	−47		0·9	1·4		4	14	16	0·088	0·092	4	R
G316·8−0·0	14 41 22	−59 35·6	−39	1·7	2·2	3·4	1·2	6	22	25	0·136	0·147	5	R
G317·0+0·3	14 41 46	−59 13·0	−48		0·9	0·8		6	9·5	12·5	0·064	0·066	6	
G322·2+0·6	15 14 45	−56 28·5	−55	0·4	1·0	1·3		2	9	10	0·130	0·140	7	R
G326·7+0·6	15 41 01	−53 57·9	−21		0·9	1·8		3	28	29·5	0·061	0·063	8	R(G)
G326·7+0·6	15 41 01	−53 57·9	−46		0·9	1·5	1·9	3	28	29·5	0·051	0·053	8	R(G)
G326·9−0·0	15 45 06	−54 16·0	−56			0·8		9	8	12·5	0·064	0·066	9	
G326·9−0·0	15 45 06	−54 16·0	−46			0·6		9	8	12·5	0·048	0·049	9	
G327·3−0·5	15 49 06	−54 27·1	−50	0·5	2·9	3·7	1·9	9	28	32·5	0·114	0·121	10	R
G332·1−0·4	16 12 47	−51 09·3	−44		1·0	1·4		7	9·5	13	0·108	0·114	11	
G332·1−0·4	16 12 47	−51 09·3	−57		0·7	0·8		7	9·5	13	0·062	0·064	11	
G332·4−0·4	16 13 37	−50 55·6	−43		1·3	0·7		7	13	16·5	0·042	0·043	12	R
G332·7−0·6	16 16 01	−50 33·3	−41			1·1		7	25	28·5	0·039	0·040	13	
G333·1−0·4	16 17 06	−50 30·8	−55			3·0	(0·9)	8	43	47	0·064	0·066		G
G333·1−0·4	16 17 06	−50 30·8	−42			2·1		8	43	47	0·045	0·046		G
G333·6−0·2	16 18 22	−49 58·5	−42	1·1	2·1	3·6		8	42	45	0·080	0·083		G
G333·6−0·2	16 18 22	−49 58·5	−53			—	2·0	8	42	45	—	—		G

(1) Continuum source number	(2) Position (1950) R.A. h m s	(3) Dec. ° ′	(4)	(5)	(6)	(7)	(8)	(9)	(10)	(11)	(12)	(13)	(14)	(15)
					OH absorption			Continuum temperature						
			V_{lsr} (km s^{-1})	T_{1612} (K)	T_{1665} (K)	T_{1667} (K)	T_{1720} (K)	T_g (K)	T_s (K)	T_c (K)	T_{1667}/T_c	τ_{1667}	Fig.	Refs[A]
G335·8−0·1	16 27 19	−48 24·0	−44		0·5	0·75		7	6	9·5	0·079	0·082	14	
G336·0+0·1	16 27 03	−48 04·0	−50			0·6		7	6	9·5	0·063	0·065	15	
G336·4−0·0	16 29 32	−47 49·0	−37			0·9		12	5	11	0·082	0·085	16	
G336·4−0·2	16 30 27	−47 56·0	−38			0·6		12	12	18	0·033	0·034	17	
G336·5−1·5	16 36 17	−48 46·0	−24			0·8		6	7	10	0·080	0·083	18	
G336·8+0·0	16 30 51	−47 31·0	−4			0·9		12	29	35	0·026	0·026	19	
G336·8+0·0	16 30 51	−47 31·0	−20			0·6		12	29	35	0·017	0·017	19	
G336·8+0·0	16 30 51	−47 31·0	−38			1·6		12	29	35	0·046	0·047	19	
G336·8+0·0	16 30 51	−47 31·0	−50			0·5		12	29	35	0·014	0·014	19	
G336·8+0·0	16 30 51	−47 31·0	−76			0·6		12	29	35	0·017	0·017	19	
G337·1−0·2	16 33 04	−47 25·0	−21		0·6	0·7		12	17	23	0·030	0·030	20	
G337·1−0·2	16 33 04	−47 25·0	−38		0·7	2·5		12	17	23	0·109	0·116	20	
G337·1−0·2	16 33 04	−47 25·0	−76		0·9	0·8		12	17	23	0·035	0·036	20	
G337·8−0·1	16 35 15	−46 52·9	−38		0·8	1·4		12	10	16	0·088	0·092	21	
G337·9−0·5	16 37 27	−47 02·0	−36		0·9	1·7		8	11	15	0·113	0·120	22	
G338·0−0·1	16 36 10	−46 41·6	−42		0·8	1·2		12	18	24	0·050	0·052	23	R
G338·0−0·1	16 36 10	−46 41·6	−89		0·5	1·0		12	18	24	0·042	0·043	23	R
G338·4+0·1	16 37 07	−46 18·6	−34		0·8	1·6		9	34	38·5	0·042	0·043	24	R
G338·4+0·1	16 37 07	−46 18·6	−77	0·6	0·7	1·3		9	34	38·5	0·034	0·035	24	R
G338·4−0·2	16 38 09	−46 29·0	−35			0·6		9	9	13·5	0·044	0·045	25	
G338·9+0·6	16 36 40	−45 35·0	−63			0·9		8	9·5	13·5	0·067	0·070	26	R
G340·3−0·2	16 45 22	−45 05·0	−40			1·0		8	5	9	0·111	0·118	27	
G340·8−1·0	16 50 44	−45 12·0	−28		0·6	0·9		5	10	12·5	0·072	0·075	28	
G345·4+1·4	16 56 04	−40 08·0	−12			1·5		4	19	21	0·071	0·074	29	
G345·4−0·9	17 05 56	−41 32·7	−22		1·2	1·5	0·8	3	19	20·5	0·073	0·076	30	R
G348·5+0·1	17 11 11	−38 26·9	−9	0·4	0·4	0·7		6	25	28	0·025	0·025	31	R
G348·7−1·0	17 16 37	−38 55·0	−13		1·1	1·7	0·5	4	29	31	0·055	0·057	32	R
G348·7−1·0	17 16 37	−38 55·0	−32	0·8	0·7	0·6		4	29	31	0·019	0·019	32	R
G351·7−1·2	17 25 58	−36 35·3	−12		1·5	1·5	1·6	4	13	15	0·100	0·106	33	R

[A] References:

M. More detailed results given by Manchester *et al.* (1970).

G. More detailed results given by Goss *et al.* (1970).

R. Preliminary report given by Robinson *et al.* (1971).

3. Results

In Table 1 we list the data on the 33 sources against which absorption was discovered in the search (including 14 for which preliminary data were given by Robinson *et al.* (1971)). In 10 cases, features at more than one velocity are present in a source, the total number of absorption features being 47.

With these new sources we have also listed in Table 1 the corresponding data for an additional 11 sources in the longitude range 265°–350°, which were studied by Goss *et al.* (1970) or Manchester *et al.* (1970). In Section 4 these data are combined with the present results to investigate the general distribution of OH absorption in this region of the Galaxy. Columns 1–8 of Table 1 are self explanatory. Columns 9 and 10 are measurements of the continuum radiation. The antenna temperatures T_s of the discrete sources were measured in most cases with a broadband continuum channel of the receiver during right ascension and declination scans through the sources. The galactic background temperatures T_g (and T_s in a few cases) were estimated from the 1410 MHz map of Hill (1968) and the maps of the Parkes 2700 MHz galactic survey, with appropriate allowance being made for spectral index.

Columns 11–13 relate to the estimation of the optical depth τ. In order to determine τ, we make the assumption that the excitation temperature of the OH equals the cosmic background isotropic radiation temperature ($\sim$3 K) and that the continuum radiation T_c being absorbed comprises the discrete source together with half of the galactic background radiation, that is, $T_c = T_s + \frac{1}{2}T_g$. Thus for an OH absorption of depth T_L, where L stands for one of the four OH transitions, we have

$$1-\exp(-\tau_L) = T_L/T_c = T_L/(T_s+\tfrac{1}{2}T_g). \quad (1)$$

Our assumption that, typically, half of the galactic background radiation originates beyond the OH absorbing cloud could be refined using distance estimates, but this was not felt to be worth while. The maximum possible error of the assumption is only $\pm\frac{1}{2}T_g$ and in most cases is quite small. Values of $\frac{1}{2}T_g$ lie between 0 and 7·5 K in antenna temperature (the corresponding full-beam brightness temperatures are larger by a factor of 1·32). The excitation temperature of the OH is not known, but estimates of it usually lie in the range 3–10 K. For comparison we note that Turner (1972), in a similar study of OH absorption (see Section 5*b* below), assumed that the excitation temperature of the OH equals the temperature of the galactic background. His values of τ were calculated from $\tau = T_L/(T_s+3)$, where brightness temperatures have been used.

The optical depth estimate (as measured by us or by Turner 1972) is an average over an area which is usually determined predominantly by the angular extent of the source. However, in the case of weak sources, the estimate approximates more nearly to the average over the antenna beam (which is usually considerably larger) because for weak sources the more diffuse background radiation is a significant contribution to the total. If the OH clouds contain dense blobs with a scale size smaller than the angular extent of the source, the values of τ determined from equation (1) will be lower limits to the peak optical depths through the blobs.

In Figs 1–33 we present profiles for each of the 33 new sources. Radial velocities are given relative to the local standard of rest. The total integration time (in minutes) is marked on each profile. In those cases where the integration time was at least

15 min, the profile is usually the average of two observations, each of half the total time, made in the two opposite senses of circular polarization. Where available, the velocity extent between half-intensity points of the H109α recombination line from the continuum source is also shown.

Table 2. Satellite-line emission accompanying 1667 MHz absorption

(1) Continuum source number	(2) Position (1950) R.A. h m s	(3) Dec. ° ′	(4) OH line (MHz)	(5) OH position (1950) R.A. h m s	(6) Dec. ° ′	(7) r.m.s. error	(8) V_{lsr} (km s^{-1})	(9) Notes[A]
G305·2+0·0	13 08 03	−62 29·2	1612	—	—	—	−40	1
G316·8−0·0	14 41 22	−59 35·6	1720	—	—	—	−38	1
G316·8−0·0	14 41 22	−59 35·6	1612	14 41 28	−59 36·8	2′·0	−35	
G326·7+0·6	15 41 01	−53 57·9	1612	15 41 02	−53 55·4	0·7	−44	
G327·3−0·5	15 49 06	−54 27·1	1612	15 49 08	−54 25·8	0·6	−47	
G327·3−0·5	15 49 06	−54 27·1	1612	15 50 16	−54 24·1	0·3	−22, +5	2
G332·1−0·4	16 12 52	−51 10·1	1612	—	—	—	−43	1
G338·0−0·1	16 36 10	−46 41·6	1612	16 36 19	−46 44·1	0·3	−88, −48	3
G338·0−0·1	16 36 10	−46 41·6	1720	—	—	—	−50	1
G338·5+0·1	16 37 07	−46 18·6	1612	16 37 28	−46 13·6	1·0	−144, −114	4
G338·9+0·6	16 36 40	−45 35·0	1612	16 36 56	−45 35·9	0·3	−62	5
G345·4−0·9	17 05 56	−41 32·5	1612	—	—	—	−22	1
G348·7−1·0	17 16 39	−38 54·6	1612	17 16 36	−38 55·0	~3·0	−12	6
G351·7−1·2	17 25 58	−36 35·3	1612	17 25 58	−36 37·8	2·0	−10	

[A] Footnotes:

1. OH source detected at search position; no additional measurements made.
2. Source displays OH/IR characteristics (OH 327·4−0·6).
3. Source displays OH/IR characteristics (OH 338·0−0·1).
4. Source displays OH/IR characteristics (OH 338·5+0·1); see Caswell *et al.* (1971).
5. OH source position is that of strong accompanying 1665 MHz emission; there is a high degree of circular polarization (see Robinson *et al.* 1971, 1974).
6. OH source probably lies within 3′ arc of discovery position.

While making satellite-line observations in the direction of sources showing main-line absorption features, we detected 14 new OH emission sources, details of which are given in Table 2. One 1612 MHz source is associated with 1665 MHz emission and three possess OH/IR characteristics; the remaining 10 (8 at 1612 MHz and 2 at 1720 MHz) appear to be associated with the main-line absorption. Although these remaining sources are quite weak we have been able to position five of them.

Table 3 lists the positions searched unsuccessfully for 1667 MHz absorption, together with the centre velocity V_0 (relative to the local standard of rest) of the radial velocity range searched; an approximate value of T_s is given from which an upper limit τ_{ul} on τ has been derived on the assumption that any absorption is weaker than 1 K (T_a).

No new 1667 MHz emission sources were detected other than those associated with previously detected stronger 1665 MHz emission. Thus W42 remains a unique object with emission so far detected at only 1667 MHz (Robinson *et al.* 1970).

4. Notes on Individual Sources

G274·0−1·1 (Fig. 1). The continuum source is a small-diameter (1′·7 × 1′·6 arc) HII region (Caswell 1972) whose H109α recombination-line velocity is +39 km s^{-1}, in good agreement with that of the single OH absorption feature.

G298·9−0·4 (Fig. 2). The absorption is broad or double but lies within the range of H109α velocities of the continuum HII region. For the feature at +19 km s^{-1}, the 1667 MHz absorption is about four times that at 1665 MHz, a departure from the expected equilibrium value of 1·8 in the opposite sense to departures commonly encountered. No feature is visible at 1720 MHz, while very weak absorption may be present at 1612 MHz.

Table 3. 72 continuum sources where no significant 1667 MHz OH absorption was detected

(1) Source	(2) T_s (K)	(3) T_c (K)	(4) τ_{ul}	(5) V_0 (km s^{-1})	(1) Source	(2) T_s (K)	(3) T_c (K)	(4) τ_{ul}	(5) V_0 (km s^{-1})
G269·2−1·4	8	9	0·11	+10	G326·2−1·7	27	28	0·04	−50
G283·6−1·0	11	12	0·08	0	G326·3+0·7	9	10	0·10	−50
G284·0−0·9	20	21	0·05	0	G326·4+0·9	9	10	0·10	−50
G286·2−0·2	13	14	0·07	0	G326·6−0·5	12	13	0·08	−50
G289·1−0·4	8	9	0·11	0	G327·3+0·4	10	12	0·08	−50
G289·8−1·1	16	17	0·06	0	G327·6−0·4	9	11	0·09	−50
G290·1−0·8	19	20	0·05	0	G327·8+0·1	10	12	0·08	−50
G291·0−0·1	11	12	0·08	0	G328·0−0·1	8	10	0·10	−50
G292·0+1·8	8	8	0·13	0	G328·3+0·4	10	12	0·08	−50
G295·0−1·7	12	12	0·08	0	G328·4+0·2	13	15	0·07	−50
G295·2−0·6	11	12	0·08	0	G331·3−0·3	14	17	0·06	−50
G298·2−0·3	25	26	0·04	0	G332·5+0·1	4	7	0·14	−50
G298·6−0·1	30	31	0·03	0	G333·0+0·8	13	16	0·06	−50
G303·4(5)−0·7	4	6	0·17	−30	G334·7−0·2	7	10	0·10	−50
G305·6+0·0	31	32	0·03	0	G334·9−0·3	8	11	0·09	−50
G307·1+1·2	6	7	0·14	0	G335·1+0·1	8	11	0·09	−50
G307·6−0·3	6	7	0·14	0	G336·7+0·5	7	10	0·10	−50
G308·7+0·1	7	8	0·13	0	G337·2−0·7	3	6	0·17	−50
G309·7+1·7	36	37	0·03	+10	G338·9−0·1	7	10	0·10	−50
G311·1−0·3	7	9	0·11	−30	G339·1−0·4	7	10	0·10	−50
G311·5+0·4	10	12	0·08	−50	G339·3+0·2	6	9	0·11	−50
G311·5−0·4	9	11	0·09	−50	G341·2−0·3	7	10	0·10	−50
G311·6−0·6	9	11	0·09	−30	G342·3+0·3	8	11	0·09	−50
G312·3−0·3	11	13	0·08	−50	G343·5−0·0	13	16	0·06	−50
G312·6+0·2	3	5	0·20	−30	G344·9+1·7	12	14	0·07	−50
G314·2+0·4	6	7	0·14	−50	G345·2+1·0	10	13	0·08	−50
G316·3−0·0	9	10	0·10	−50	G345·0+1·5	13	15	0·07	−50
G317·3+0·3	8	10	0·10	−50	G345·2−0·8	5	7	0·14	−50
G319·2−0·3	7	8	0·13	−50	G345·6−0·0	12	15	0·07	−50
G319·4+0·0	5	6	0·17	−50	G346·2−0·1	7	10	0·10	−50
G320·2+0·8	6	7	0·14	−50	G346·6−0·2	5	8	0·13	−50
G320·3−0·2	9	10	0·10	−50	G347·6+0·2	12	15	0·07	−50
G320·3−0·3	9	10	0·10	−50	G348·2−1·0	7	10	0·10	−50
G320·3−1·0	14	15	0·07	−50	G348·6−0·6	8	11	0·09	−50
G321·1−0·5	9	10	0·10	−50	G349·8−0·6	7	10	0·10	−50
G324·2+0·2	4	5	0·20	−50	G349·7+0·2	12	15	0·07	−50

G305·2+0·0 (Fig. 3). The H109α velocity of the continuum source spans the velocity of the broad or double OH absorption feature. Although weak, a broad 1612 MHz emission feature is probably real and coincides in velocity with the 1667 MHz absorption.

Figs 1–33 (pp. 603–20). Profiles of OH absorption for the indicated continuum sources. The filter bandwidth is 10 kHz and the velocity extent between half-intensity points of H109α recombination-line emission from the continuum source is shown. Radial velocities are given relative to the local standard of rest. Fig. 10A is an exception in that it shows the 1612 MHz emission profile of the OH/IR source OH 327·4−0·6 discovered near G327·3−0·5 (which is shown in Fig. 10).

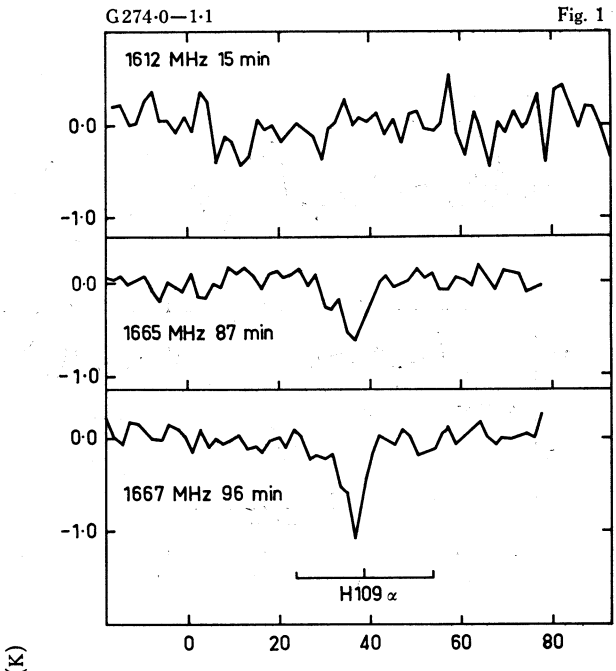
G 274·0—1·1
1612 MHz 15 min
0·0
-1·0
0·0
1665 MHz 87 min
-1·0
0·0
1667 MHz 96 min
-1·0
H109 α
0
20
40
60
80

Fig. 1

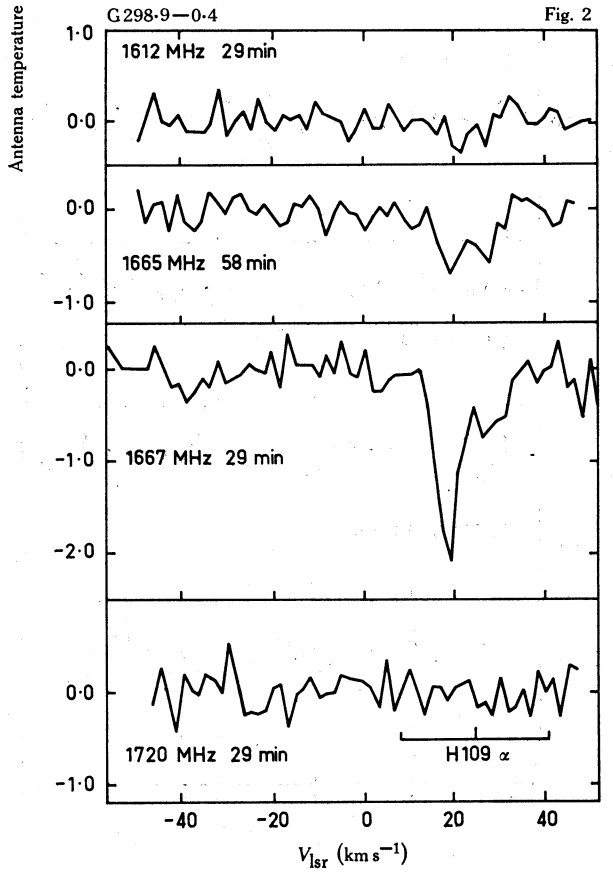
G 298·9—0·4
1612 MHz 29 min
1·0
0·0
0·0
1665 MHz 58 min
-1·0
0·0
-1·0
1667 MHz 29 min
-2·0
0·0
1720 MHz 29 min
H109 α
-1·0
-40
-20
0
20
40
Antenna temperature (K)
V_{lsr} (km s^{-1})

Fig. 2

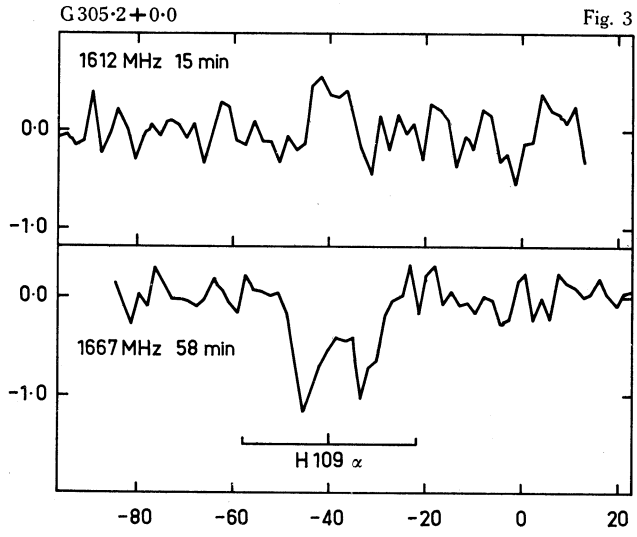
G 305·2+0·0
1612 MHz 15 min
0·0
-1·0
0·0
1667 MHz 58 min
-1·0
H 109 α
-80
-60
-40
-20
0
20

Fig. 3

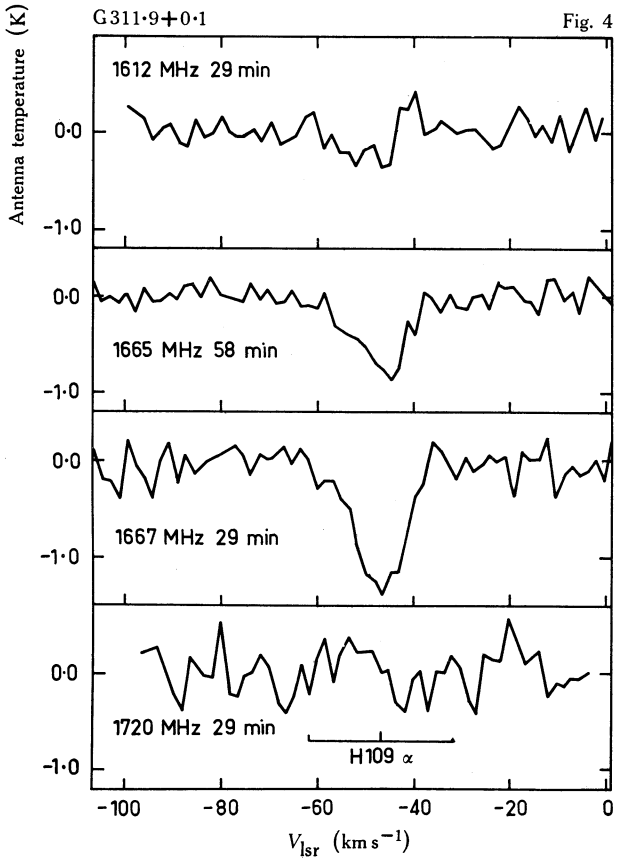
G 311·9+0·1
1612 MHz 29 min
0·0
-1·0
0·0
1665 MHz 58 min
-1·0
0·0
1667 MHz 29 min
-1·0
0·0
1720 MHz 29 min
H109 α
-1·0
-100
-80
-60
-40
-20
0
Antenna temperature (K)
V_{lsr} (km s^{-1})

Fig. 4

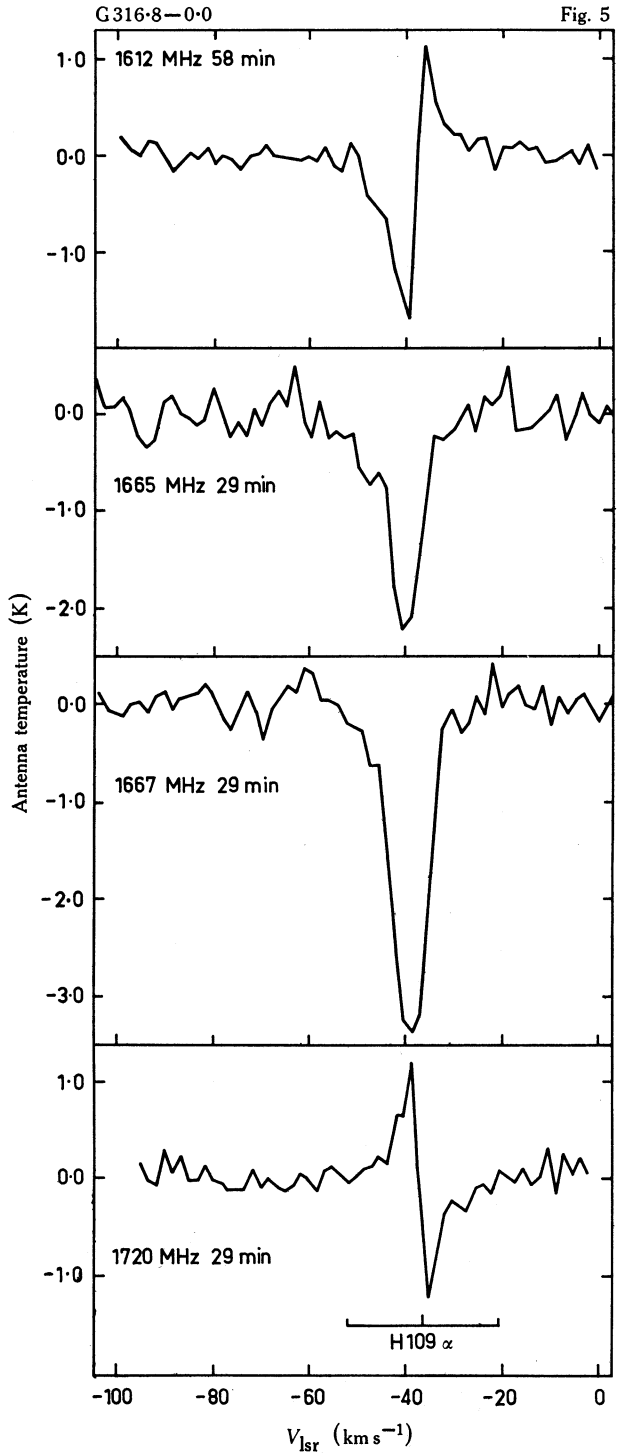
G 316·8—0·0
Fig. 5
1612 MHz 58 min
1665 MHz 29 min
1667 MHz 29 min
1720 MHz 29 min
H109 α
Antenna temperature (K)
V_{lsr} (km s^{-1})

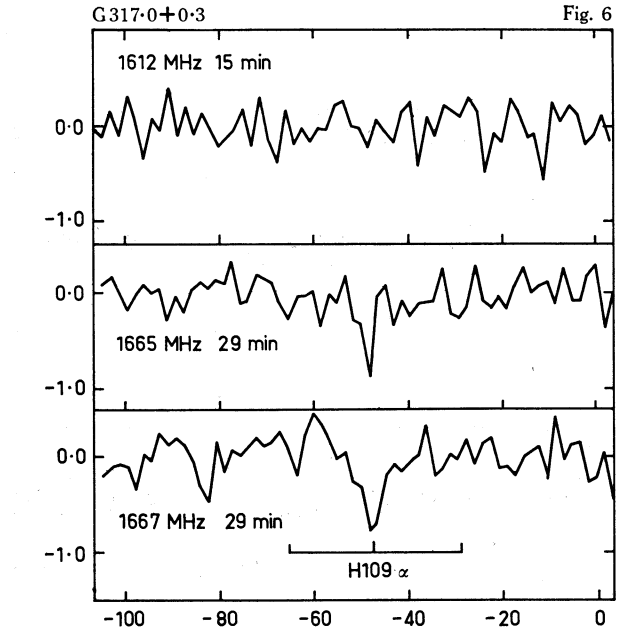
G317·0+0·3
1612 MHz 15 min
1665 MHz 29 min
1667 MHz 29 min
H109 α
0·0
-1·0
-100
-80
-60
-40
-20
0

Fig. 6

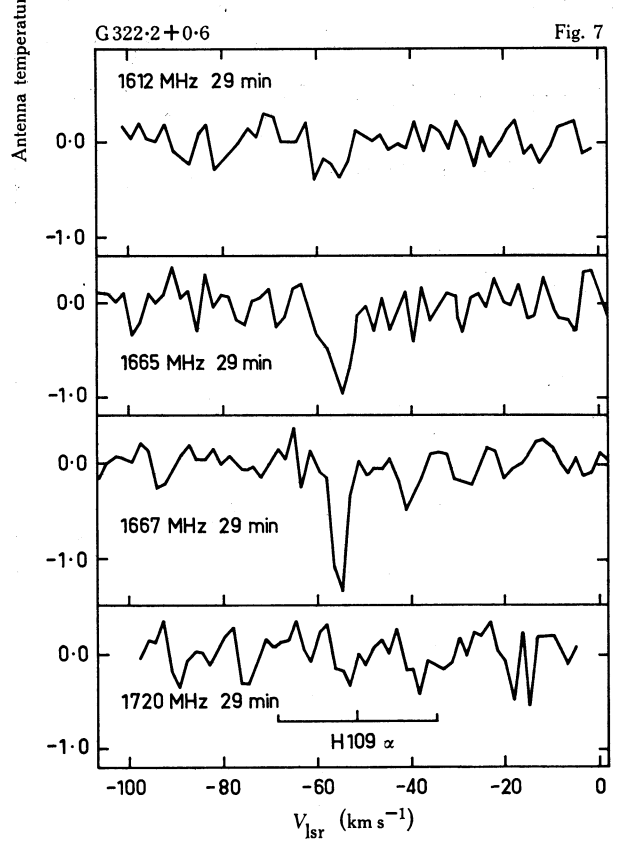
G322·2+0·6
1612 MHz 29 min
1665 MHz 29 min
1667 MHz 29 min
1720 MHz 29 min
H109 α
Antenna temperature (K)
0·0
-1·0
-100
-80
-60
-40
-20
0
V_{lsr} (km s^{-1})

Fig. 7

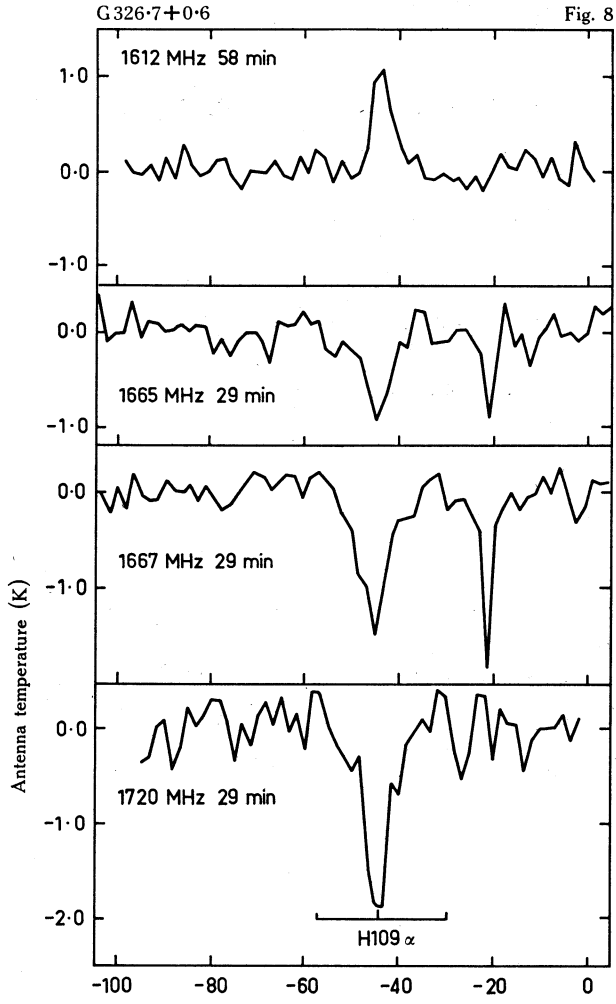
G 326·7+0·6
1612 MHz 58 min
1665 MHz 29 min
1667 MHz 29 min
1720 MHz 29 min
H109 α
Antenna temperature (K)
1·0
0·0
-1·0
-2·0
-100
-80
-60
-40
-20
0

Fig. 8

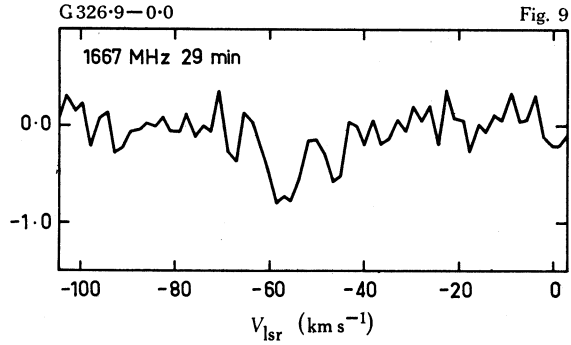
G 326·9−0·0
1667 MHz 29 min
0·0
-1·0
-100
-80
-60
-40
-20
0
V_{lsr} (km s^{-1})

Fig. 9

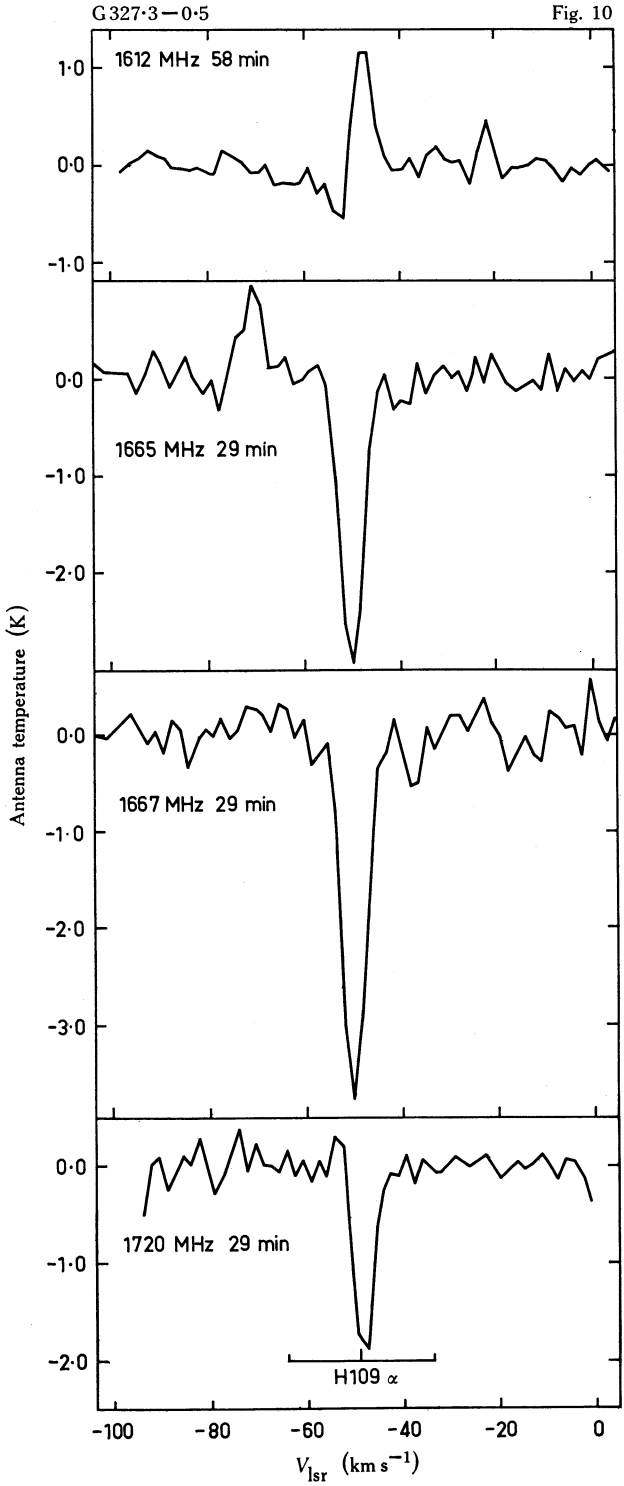
G 327·3 — 0·5
Fig. 10
1612 MHz 58 min
1665 MHz 29 min
1667 MHz 29 min
1720 MHz 29 min
H109 α
Antenna temperature (K)
V_{lsr} (km s^{-1})

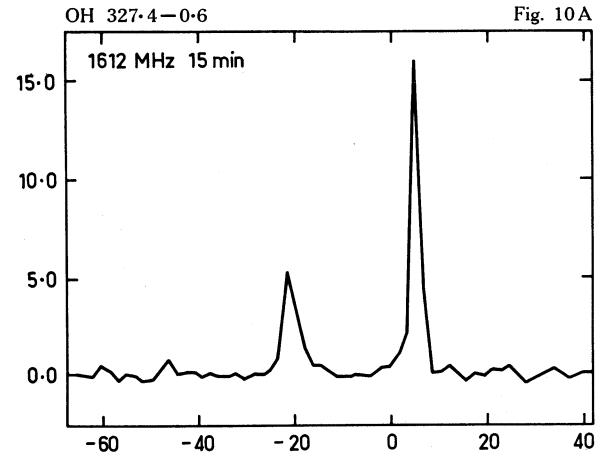
OH 327·4−0·6
Fig. 10A
1612 MHz 15 min
15·0
10·0
5·0
0·0
-60
-40
-20
0
20
40

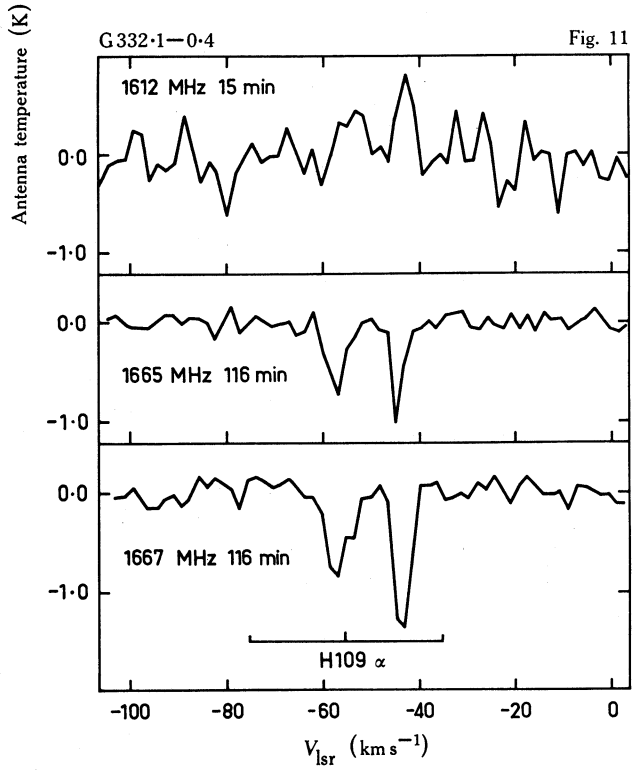
G 332·1−0·4
Fig. 11
Antenna temperature (K)
1612 MHz 15 min
0·0
-1·0
1665 MHz 116 min
1667 MHz 116 min
H109 α
-100
-80
-60
-40
-20
0
V_{lsr} (km s^{-1})

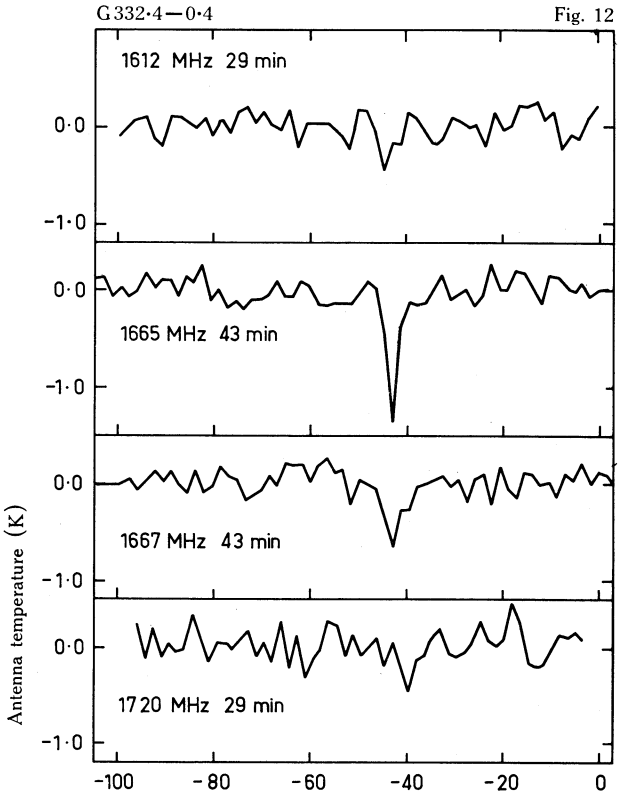
G 332·4—0·4
1612 MHz 29 min
1665 MHz 43 min
1667 MHz 43 min
1720 MHz 29 min
0·0
-1·0
Antenna temperature (K)
-100
-80
-60
-40
-20
0

Fig. 12

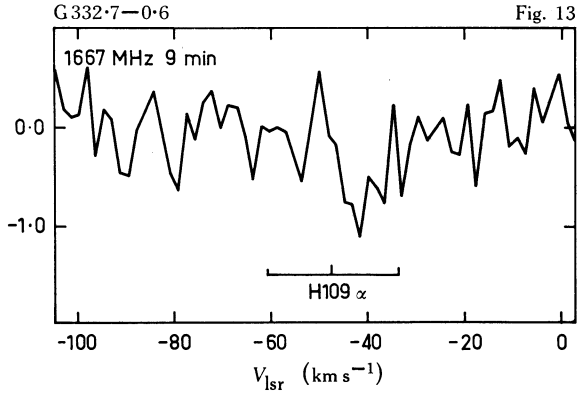
G 332·7—0·6
1667 MHz 9 min
0·0
-1·0
H109 α
-100
-80
-60
-40
-20
0
V_{lsr} (km s^{-1})

Fig. 13

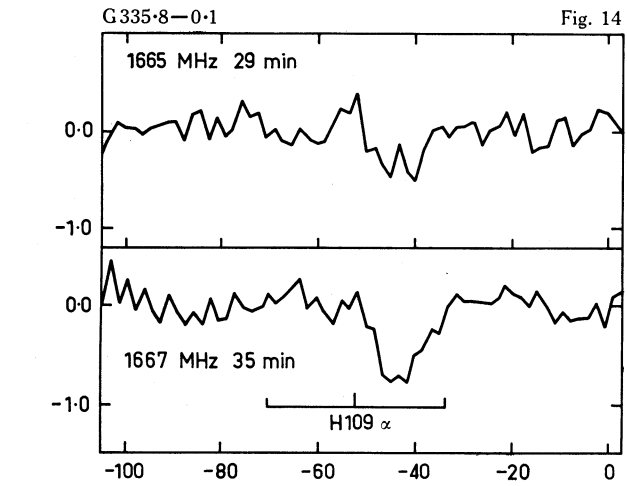

Fig. 14

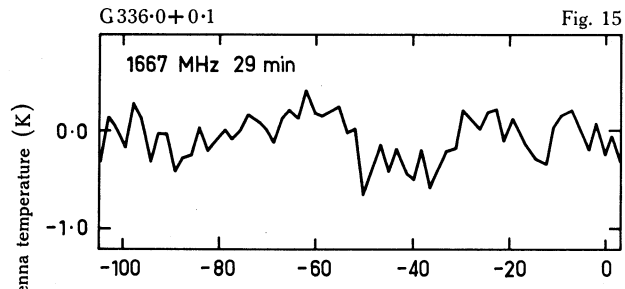

Fig. 15

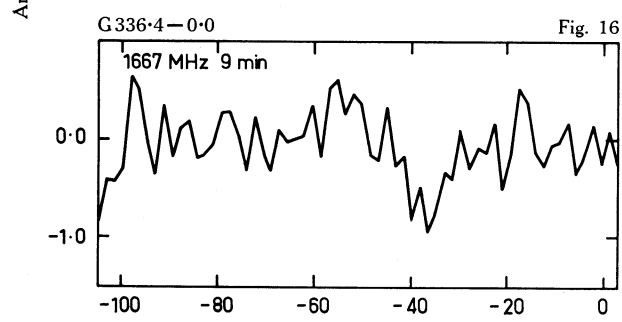

Fig. 16

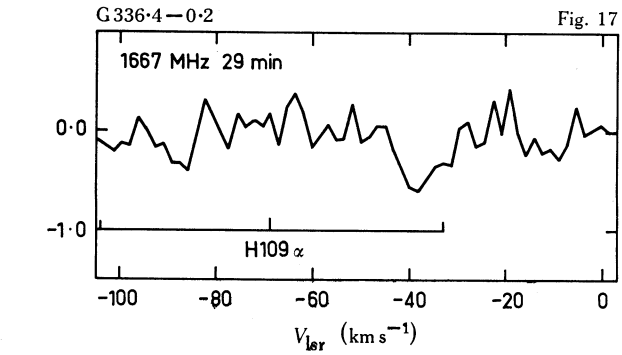

Fig. 17

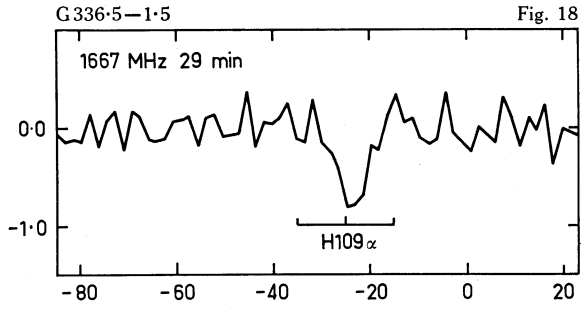

Fig. 18

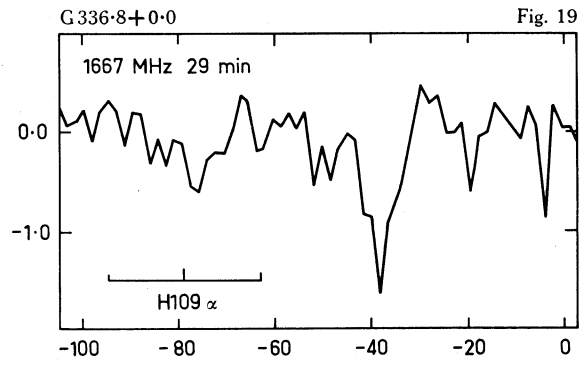

Fig. 19

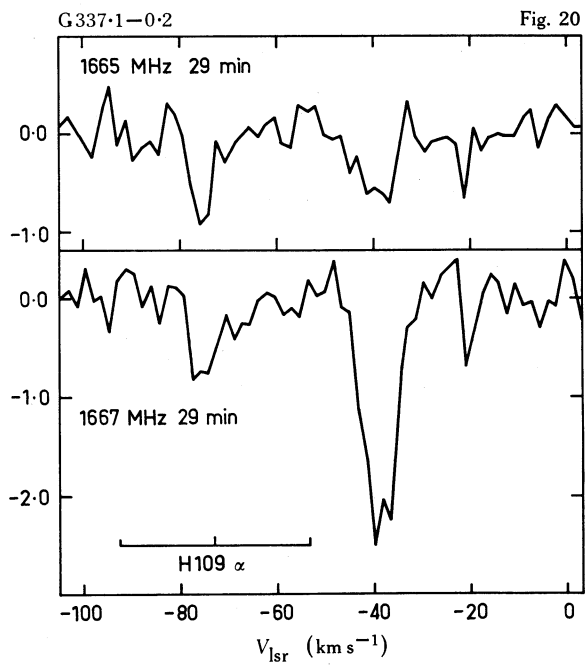

Fig. 20

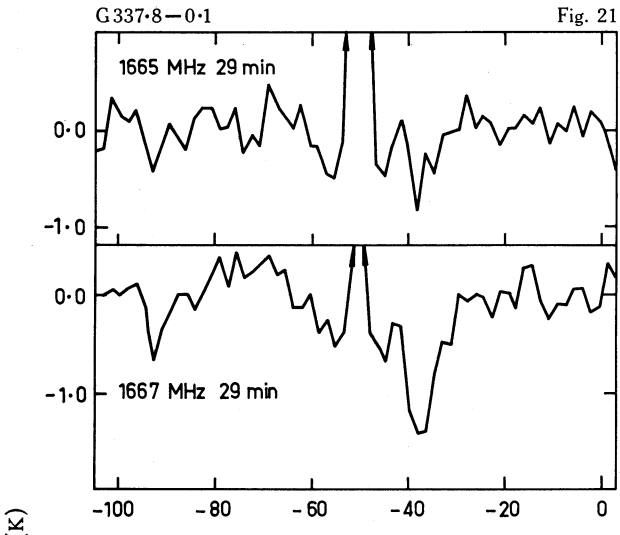
G 337·8—0·1
1665 MHz 29 min
0·0
-1·0
0·0
-1·0
1667 MHz 29 min
-100
-80
-60
-40
-20
0

Fig. 21

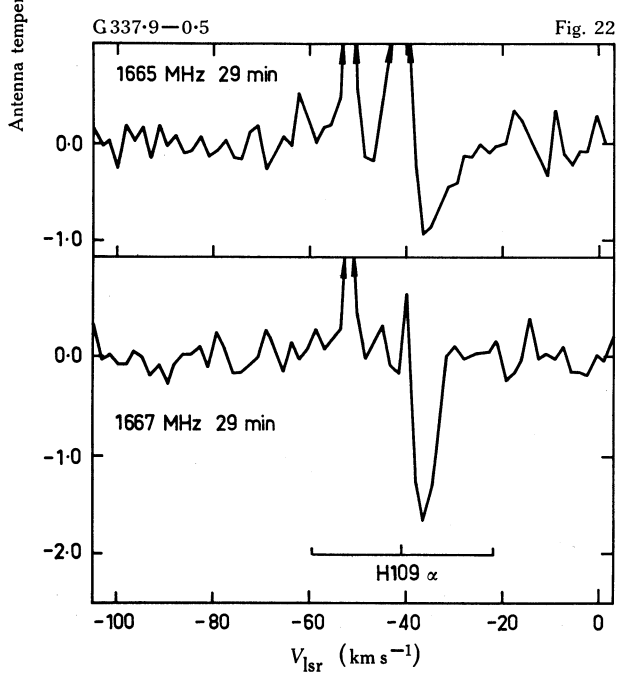
G 337·9—0·5
1665 MHz 29 min
0·0
-1·0
0·0
1667 MHz 29 min
-1·0
-2·0
H109 α
-100
-80
-60
-40
-20
0
Antenna temperature (K)
V_{lsr} (km s^{-1})

Fig. 22

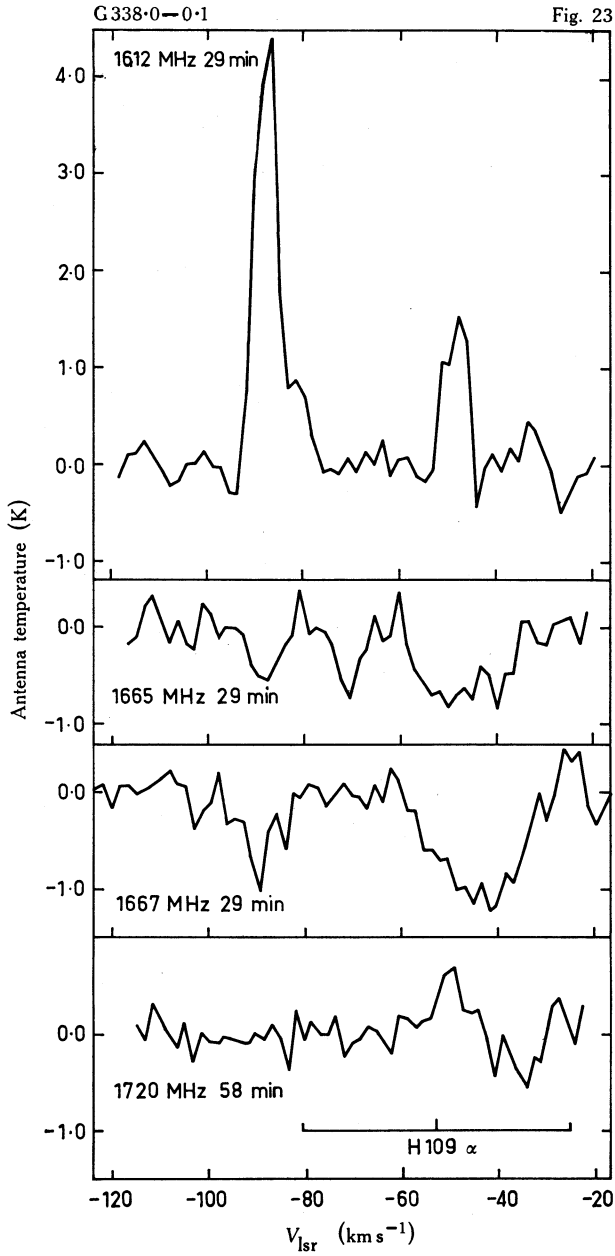
G338·0—0·1
Fig. 23
1612 MHz 29 min
1665 MHz 29 min
1667 MHz 29 min
1720 MHz 58 min
H 109 α
Antenna temperature (K)
4·0
3·0
2·0
1·0
0·0
-1·0
-120
-100
-80
-60
-40
-20
V_{lsr} (km s^{-1})

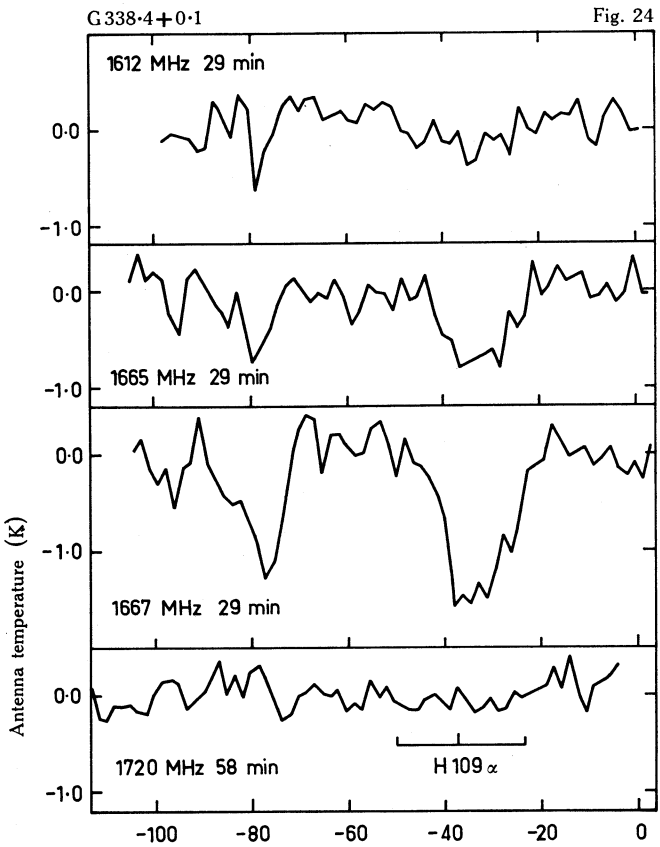
G 338·4+0·1
1612 MHz 29 min
1665 MHz 29 min
1667 MHz 29 min
1720 MHz 58 min
H 109 α
0·0
-1·0
Antenna temperature (k)
-100
-80
-60
-40
-20
0

Fig. 24

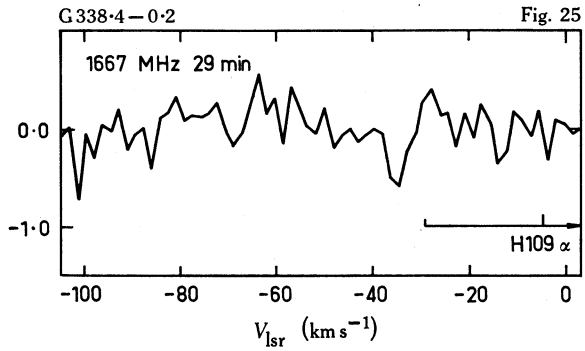
G 338·4 − 0·2
1667 MHz 29 min
H109 α
0·0
-1·0
-100
-80
-60
-40
-20
0
V_{lsr} (km s^{-1})

Fig. 25

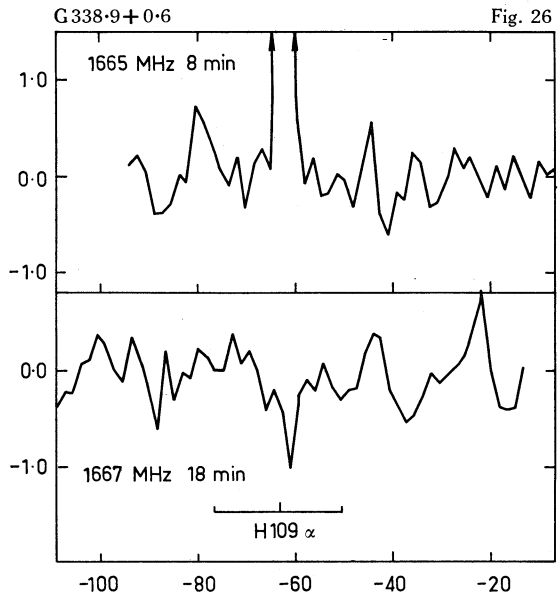

Fig. 26

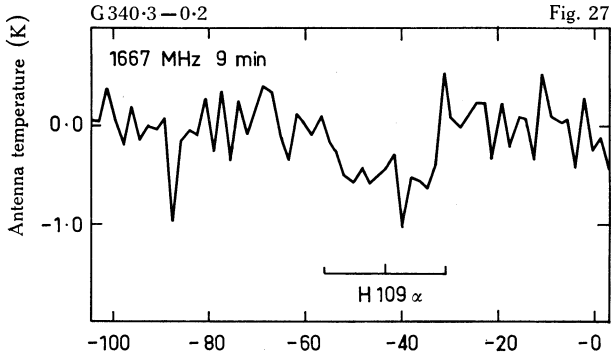

Fig. 27

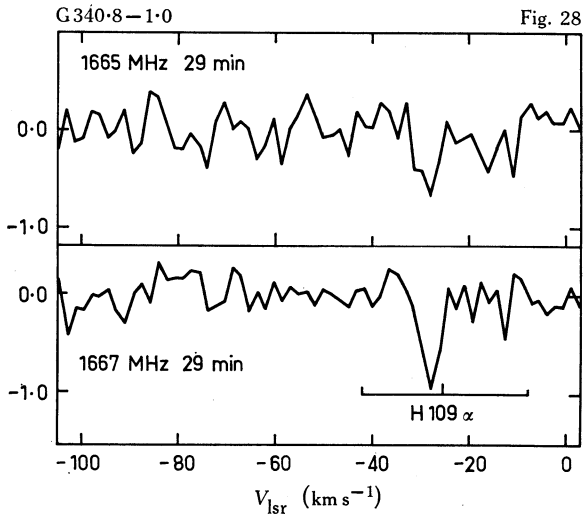

Fig. 28

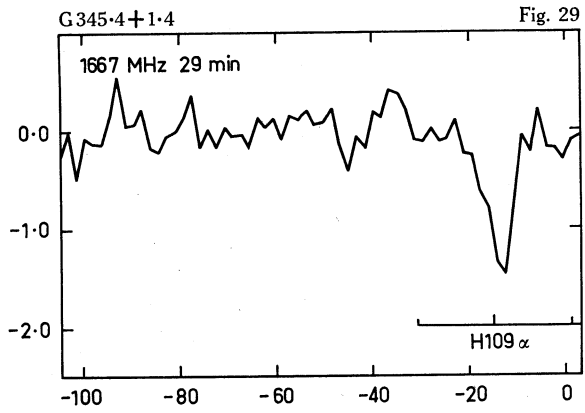
G345·4+1·4
1667 MHz 29 min
0·0
-1·0
-2·0
H109 α
-100
-80
-60
-40
-20
0

Fig. 29

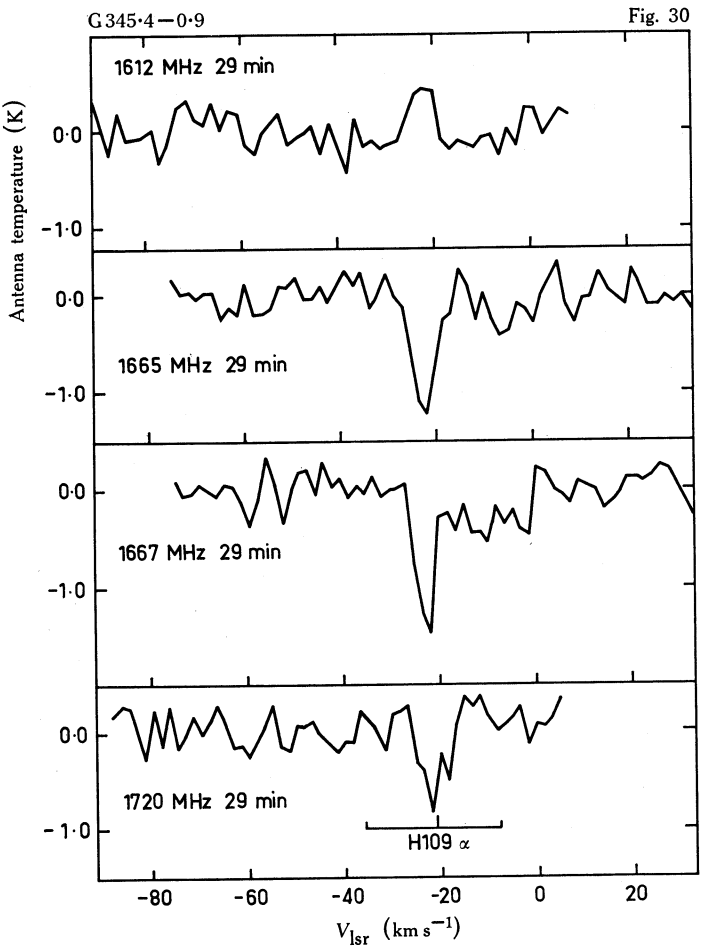
G345·4−0·9
1612 MHz 29 min
1665 MHz 29 min
1667 MHz 29 min
1720 MHz 29 min
H109 α
Antenna temperature (K)
0·0
-1·0
-80
-60
-40
-20
0
20
V_{lsr} (km s^{-1})

Fig. 30

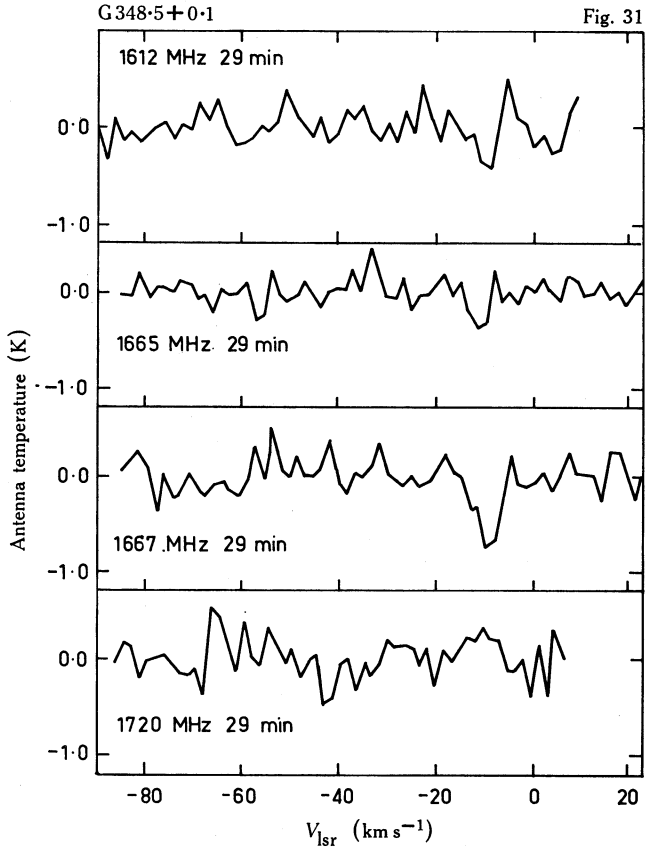
G348·5+0·1
1612 MHz 29 min
1665 MHz 29 min
1667 MHz 29 min
1720 MHz 29 min
0·0
-1·0
Antenna temperature (K)
-80
-60
-40
-20
0
20
V_{lsr} (km s^{-1})

Fig. 31

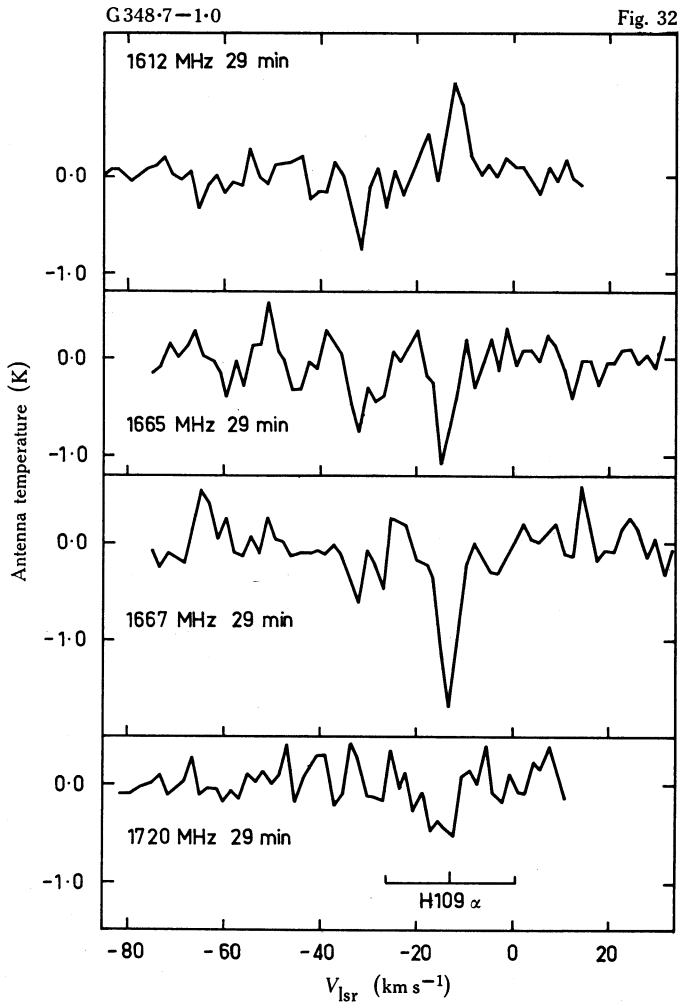
G348·7−1·0
Fig. 32
1612 MHz 29 min
1665 MHz 29 min
1667 MHz 29 min
1720 MHz 29 min
H109 α
0·0
-1·0
Antenna temperature (K)
-80
-60
-40
-20
0
20
V_{lsr} (km s^{-1})

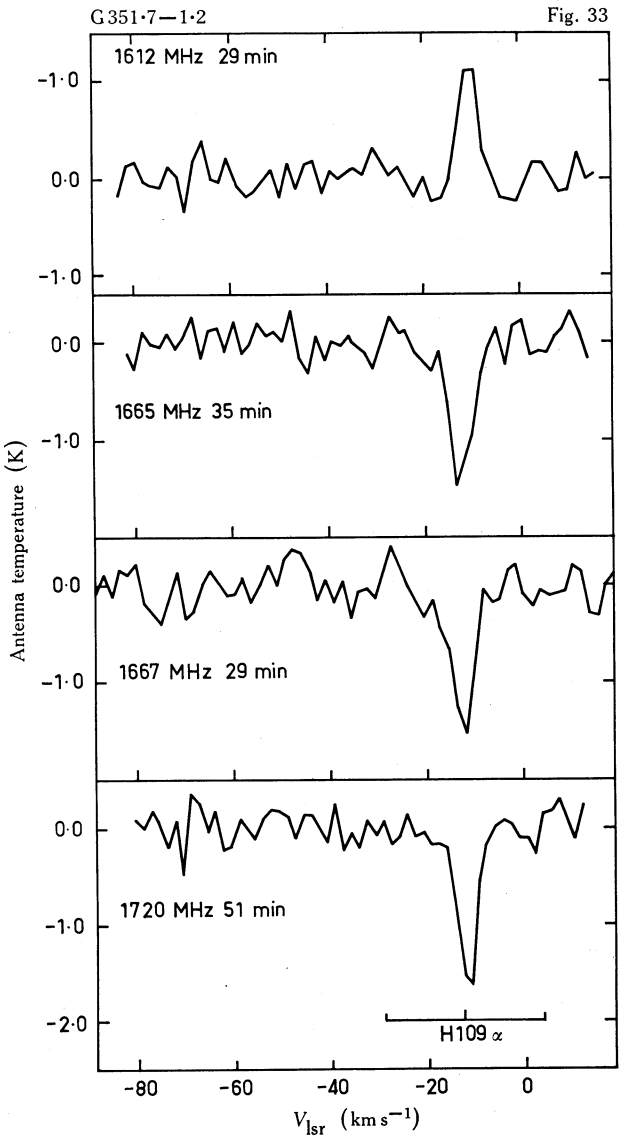
G 351·7—1·2
Fig. 33
1612 MHz 29 min
1665 MHz 35 min
1667 MHz 29 min
1720 MHz 51 min
H109 α
Antenna temperature (K)
-1·0
0·0
-1·0
0·0
-1·0
0·0
-1·0
-2·0
-80
-60
-40
-20
0
V_{lsr} (km s^{-1})

G311·9+0·1 (Fig. 4). The broad OH absorption evident at 1665 and 1667 MHz agrees well with the H109α velocity. At 1612 MHz there is weak absorption over most of this broad velocity range.

G316·8−0·0 (Fig. 5). At 1665 and 1667 MHz the absorption has depths approximately in the ratio 5 : 9 and agrees in velocity with the H109α emission. At 1612 MHz, absorption is present at the low-velocity side and emission at the high-velocity side whereas, at 1720 MHz, emission is present at the low-velocity side and absorption at the high-velocity side. Only the position of the 1612 MHz emission has been measured (see Table 2).

G317·0+0·3 (Fig. 6). The present signal-to-noise ratio is poor for this weak feature but its presence is evident at both 1665 and 1667 MHz and its velocity agrees well with the H109α velocity.

G322·2+0·6 (Fig. 7). At 1665 and 1667 MHz the absorption agrees well with the H109α velocity. Weak absorption may be present at 1612 MHz.

G326·7+0·6 (Fig. 8). Absorption features at two distinct velocities are present at both 1665 and 1667 MHz. Near $V = -45$ km s^{-1}, which is the H109α median velocity, anomalously strong 1720 MHz absorption occurs (1665, 1667 and 1720 MHz absorption approximately in the ratio 1 : 1·5 : 1·9) while emission occurs at 1612 MHz. At $V = -21$ km s^{-1} a very narrow absorption feature (width to half-optical-depth of less than 10 kHz, or less than 1·8 km s^{-1}) is present at both 1665 and 1667 MHz.

G326·9−0·0 (Fig. 9). The weak absorption observed at 1667 MHz has a velocity within the range of recombination-line velocities of HII regions at nearby galactic longitudes.

G327·3−0·5 (Fig. 10). The prominent absorption at 1665 and 1667 MHz has a velocity of -50 km s^{-1}, similar to that of H109α emission. At 1720 MHz the absorption is anomalously strong while at 1612 MHz there is accompanying emission. Both satellite-line features are centred at a velocity ~ 2 km s^{-1} more positive than the main-line features. The 1665 MHz emission feature near $V = -70$ km s^{-1} (due to an OH emission source 2′ arc from the peak of the HII region) is discussed more appropriately in Paper 1 since it is typical of main-line emission associated with HII regions. This feature also has associated water vapour emission at $V = -60$ km s^{-1} (Johnston *et al.* 1972). The 1612 MHz emission at $V = -22$ km s^{-1} is one of the two velocity peaks displayed by OH 327·4−0·6, shown fully in Fig. 10A. Its position (see Table 2) is displaced approximately 10′ arc from the HII region and it appears to be of the OH/IR type and unrelated to either the continuum source or the OH absorbing cloud.

G332·1−0·4 (Fig. 11). Two distinct absorption features are present at both 1665 and 1667 MHz. One feature with $V = -57$ km s^{-1} agrees in velocity with the median value of the H109α emission. The feature at $V = -44$ km s^{-1} is within the range of the H109α emission but is quite distinct and is somewhat narrower. The 1612 MHz profile shows emission at $V = -43$ km s^{-1}, and the weaker emission near $V = -55$ km s^{-1} may also be real since it is broad and coincides in velocity with the main-line absorption.

G332·4−0·4 (Fig. 12). The continuum source shows no H109α emission and is believed to be a supernova remnant (RCW 103). The OH absorption is unusual

in being more intense at 1665 than at 1667 MHz. No satellite-line emission was detected. The velocity $V = -43\ \mathrm{km\,s^{-1}}$ corresponds to near and far kinematic distances of 3·2 and 14·5 kpc respectively. However, the same, or a related OH cloud is also seen (at the same velocity) against the adjacent sources G332·1−0·4 and G332·7−0·6, and an optical identification of the latter enables us to reject the far distance (see the following subsection). We thus adopt $3{\cdot}2 \pm 0{\cdot}7$ kpc as the distance of the OH absorbing cloud. This error corresponds to an allowance for deviations of $\pm 10\ \mathrm{km\,s^{-1}}$ from Schmidt's (1965) rotation model. Therefore 3·2 kpc is a lower limit to the distance of RCW 103. The unusual line intensity ratio may be attributable to the physical proximity of the supernova remnant and the OH cloud, in which case 3·2 kpc would represent an actual distance estimate for RCW 103. Westerlund's (1969) photometric distance of 3·9 kpc for the OB association to which RCW 103 may belong is in quite good agreement with our value.

G332·7−0·6 (Fig. 13). Our short integration time, although not providing a good signal-to-noise ratio, is adequate to demonstrate a feature at $V = -41\ \mathrm{km\,s^{-1}}$. This may be caused by the same single extended cloud of OH which is seen against the preceding two sources. The continuum source corresponds optically to RCW 106, which Shaver and Goss (1970) suggest is 3·5 kpc distant (adopting the near kinematic distance and rejecting the far value on account of the high optical luminosity).

G335·8−0·1, G336·0+0·1, G336·4−0·0 and G336·4−0·2 (Figs 14–17). Despite quite low signal-to-noise ratios, broad absorption features near $V = -40\ \mathrm{km\,s^{-1}}$ are evident for each source. The angular separations of the sources are sufficiently small to suggest that the absorption is caused by a single very extensive OH cloud. In only two cases are there H109α observations: for G335·8−0·1 the H109α velocity is slightly offset from the OH velocity, while for G336·4−0·2 the offset is considerable but the H109α velocity width reported by Wilson *et al.* (1970) is unusually large.

G336·5−1·5 (Fig. 18). This HII region corresponds to RCW 108 and is well separated from the galactic plane; its H109α velocity agrees well with that of the OH absorption.

G336·8+0·0 and G337·1−0·2 (Figs 19 and 20). These adjacent HII regions have H109α velocities centred at −79 and $-73\ \mathrm{km\,s^{-1}}$ respectively. Both show OH absorption over this velocity range and both show more prominent absorption near $V = -40\ \mathrm{km\,s^{-1}}$. Near $V = -20\ \mathrm{km\,s^{-1}}$ weak absorption is detected against both sources.

G337·8−0·1 and G337·9−0·5 (Figs 21 and 22). The source G337·9−0·5 is thermal, with H109α emission centred at $V = -40\ \mathrm{km\,s^{-1}}$, while G337·8−0·1 is predominantly nonthermal and shows no recombination line. OH emission sources are superimposed on each profile (Fig. 21: at $V = -50\ \mathrm{km\,s^{-1}}$ we see emission from OH 337·7−0·1, which is 7′ arc from the continuum source; Fig. 22: at $V = -42$ and $-52\ \mathrm{km\,s^{-1}}$ we see emission from OH 337·9−0·5, which is less than 1′ arc from the HII region) and these are discussed fully in Paper 1. The angular separation of the two continuum sources is small and both show OH absorption near $V = -38\ \mathrm{km\,s^{-1}}$, close to the velocity of one of the absorption features detected against the two preceding sources. The weak absorption near $V = -93\ \mathrm{km\,s^{-1}}$ seen in G337·8−0·1 occurs at both 1665 and 1667 MHz, suggesting that it is probably real.

G338·0−0·1 (Fig. 23). At 1665 and 1667 MHz a very broad OH absorption feature extends from −30 to −60 km s^{-1} and corresponds quite well to the broad H109α emission. At both 1665 and 1667 MHz a narrower absorption feature is evident near $V = -89$ km s^{-1}, while an additional absorption feature near $V = -70$ km s^{-1} is present only at 1665 MHz. Assuming strict circular motions according to the Schmidt (1965) model rotation curve, we find that the HII region velocity of −52·5 km s^{-1} corresponds to near and far kinematic distances of 4·3 and 14·2 kpc respectively, while the more negative velocity OH cloud (near $V = -89$ km s^{-1}) has a kinematic distance of at least 7·0 kpc, which indicates that the near distance of the HII region should be rejected. A similar situation occurs in the nearby source G338·4+0·1 (see the following subsection), where the OH absorption again requires the adoption of the far kinematic distance. At 1720 MHz, absorption and emission are both present between −30 and −60 km s^{-1}, but there are no features corresponding to the other main-line absorption velocities.

At 1612 MHz, emission features are seen at −48 and −88 km s^{-1}, the positions of which are probably coincident since their mutual separation of less than 30″ arc in each coordinate is not significant compared with our estimated r.m.s. error of 15″ arc in their relative positions. In view of the double-peaked velocity structure, the separation and width of the peaks, the absence of detectable circular polarization, and the absence of strong accompanying emission on the main lines, we conclude that the two 1612 MHz emission features represent a single object of the OH/IR type, which we designate OH 338·0−0·1 (see Table 2). The angular extent of an OH/IR object similar to those studied in detail (e.g. NML Cyg as observed by Davies *et al.* (1972)) is expected to be several seconds of arc at most and thus is not sufficient to obscure a fraction of the continuum source large enough to account for the observed main-line absorption. Thus the coincidence in position and velocity of the two 1612 MHz emission peaks with the features seen on the other transitions is probably due to chance alone. Recent OH surveys at 1612 MHz (Winnberg *et al.* 1973; unpublished data of one of us (J.L.C.) and R. F. Haynes) show that 1612 MHz OH emitters of the OH/IR type are quite common in the galactic plane. This also argues against there being any significance in the coincidence noted here.

G338·4+0·1 (Fig. 24). Broad absorption at 1665 and 1667 MHz, probably accompanied by weak 1612 MHz absorption, is present at $V = -34$ km s^{-1}, in agreement with the H109α velocity of −36·9 km s^{-1}. A narrower absorption feature on these three transitions is present near $V = -80$ km s^{-1}, with some suggestion of accompanying 1720 MHz emission. As with the preceding source, the presence of absorption at a velocity significantly more negative than the H109α velocity shows that for the HII region the far kinematic distance (15·3 kpc) should be adopted rather than the near kinematic distance (3·2 kpc).

During our investigation of this source we found a new object of the OH/IR type, OH 338·5+0·1 (see Table 2), showing 1612 MHz emission peaks at $V = -114$ and −144 km s^{-1}. This object has been discussed more fully by Caswell *et al.* (1971).

G338·4−0·2 (Fig. 25). The velocity of the weak 1667 MHz absorption is −35 km s^{-1}, similar to that of the preceding source. Because the H109α velocity of −4 km s^{-1} reported by Wilson *et al.* (1970) is unusual for this galactic longitude, it was redetermined by one of us (J.L.C.). The H109α profile appears very broad and is probably double, with features at −44 km s^{-1} (width 36 km s^{-1}) as well as

at $-2\,\mathrm{km\,s^{-1}}$ (width $30\,\mathrm{km\,s^{-1}}$). The latter feature may correspond to a more local HII region superposed on the distant one.

G338·9+0·6 (Fig. 26). The 1667 MHz absorption at $V = -61\,\mathrm{km\,s^{-1}}$ agrees well in velocity with the H109α value. Emission at 1665 MHz obscures any possible absorption on this transition. Emission at 1612 MHz is also present, apparently related to the 1665 MHz emission. Emissions on both transitions show high degrees of circular polarization, and these are discussed more fully in Paper 1 in the context of 1665 MHz emission sources associated with HII regions. Weak 1720 MHz emission at $V = -64\,\mathrm{km\,s^{-1}}$ is noted in Paper 1 and may be associated with the 1667 MHz absorption.

G340·3−0·2 (Fig. 27). The broad 1667 MHz absorption feature near $V = -40\,\mathrm{km\,s^{-1}}$ agrees well in velocity with H109α emission. An improved signal-to-noise ratio is necessary before we can be certain that the feature near $V = -87\,\mathrm{km\,s^{-1}}$ is real; if so, it would indicate that for the HII region the far kinematic distance of 14·9 kpc should be adopted rather than the near distance of 3·9 kpc.

G340·8−1·0 (Fig. 28). The major absorption feature is at $V = -28\,\mathrm{km\,s^{-1}}$ and agrees well with the H109α velocity.

G345·4+1·4 (Fig. 29). Prominent absorption at $V = -12\,\mathrm{km\,s^{-1}}$ coincides with the H109α emission. Turner (1970) has also reported OH absorption of this source.

G345·4−0·9 (Fig. 30). Absorption at 1665, 1667 and 1720 MHz near $V = -22\,\mathrm{km\,s^{-1}}$ is accompanied by 1612 MHz emission, the velocity agreeing well with the H109α velocity of this compact HII region (Caswell 1972). There is weaker main-line absorption in the velocity range 0 to $-10\,\mathrm{km\,s^{-1}}$.

G348·5+0·1 (CTB 37A) (Fig. 31). Although weak, the absorption near $V = -10\,\mathrm{km\,s^{-1}}$ is apparent at 1612, 1665 and 1667 MHz. The source is nonthermal and shows no recombination line.

G348·7−1·0 (Fig. 32). The major absorption at $V = -13\,\mathrm{km\,s^{-1}}$ is visible at 1665, 1667 and 1720 MHz, the velocity agreeing well with the H109α velocity; 1612 MHz emission is present at this velocity. A weaker absorption feature near $V = -32\,\mathrm{km\,s^{-1}}$ is present at 1612, 1665 and 1667 MHz.

G351·7−1·2 (Fig. 33). Prominent absorption on the main lines, 1665 and 1667 MHz, was first reported by Downes (1970). Comparable absorption is present at 1720 MHz while emission occurs at 1612 MHz. The continuum source has two components (Caswell 1972) and the position of 1612 MHz emission (Table 2) agrees closely with the peak of the more intense continuum component. The depth of 2·4 f.u. for the 1667 MHz absorption measured with the present 12′ arc beam is the same as that measured by Downes with a 30′ arc beam, which suggests that absorption occurs only over a region small compared with our beam. At 1667 MHz we obtained a lower continuum flux density than that estimated by Downes from 2695 MHz data, and consequently we derive a higher value of optical depth. Turner (1970) measured a smaller absorption depth of 1·6 f.u. and suggested that Downes had overestimated τ, but we agree with Downes that τ is significantly above the median value for other clouds.

5. Discussion

(*a*) *Properties of individual sources*

Comparison of Features on Four Transitions

Where the signal-to-noise level was adequate, we have commented on the line intensity ratios in the notes on the sources in Section 4, both in cases where the ratios approximate reasonably well to the thermal equilibrium values (1 : 5 : 9 : 1 for I_{1612} : I_{1665} : I_{1667} : I_{1720}) and where they clearly violate the thermal equilibrium values, including the special cases of satellite-line emission (which may, however, arise from only a portion of the cloud detected as a main-line absorber). Even where the intensity ratios superficially match the thermal equilibrium values, there are sometimes indications that the correspondence of velocity structure is not precise. Higher sensitivity and velocity resolution are desirable to investigate this further.

As indicated in Section 4, we regard the three detected OH/IR objects as chance discoveries not related to the main-line absorption features, while OH 338·9+0·6 is associated with a 1665 MHz OH emission source. However, the remaining satellite-line emission features appear to arise from the same clouds which are seen in absorption on the main lines. They are quite weak and consequently their angular extents, positions and polarization are difficult to determine reliably. No clear evidence of significant angular extent was found, which places upper limits of $\sim 6'$ arc on the strongest sources.

Polarization

For most of the detected absorption features, equal integration times were spent on each sense of circular polarization. No significant difference was found between RH and LH senses of polarization. The satellite-line emission features likewise showed no evidence of significant circular polarization.

Association with HII Regions

Most of the continuum sources searched were HII regions. The measurements were taken at the continuum peak of each source but no attempt has been made to map the optical-depth variation across the source since in most cases our angular resolution is inadequate. Hydrogen (H109α) recombination-line velocities are available for most of the HII regions. Usually the most prominent OH absorption lies within the velocity range covered by the half-intensity width of the H109α line, although this might merely be a manifestation of their occurrence in the same spiral arms. Certainly there are a number of additional OH absorption features which do not coincide in velocity with the HII region against which they are observed, as is clear from the absorption profiles in which the extent of H109α emission is indicated. Another instance of OH absorption not being associated with an HII region is where the OH absorption occurs against a nonthermal source. However, it is worth noting that all of the detected satellite-line emission occurs in the direction of HII regions and also coincides in velocity with that of the HII regions. For comparison, we note that 'anomalous OH emission on the main lines frequently appears to be intimately associated with individual HII regions' (see Paper 1) and this link is more likely caused by the excitation mechanism than by the occurrence of high densities of OH exclusively in such regions.

(*b*) *General properties of OH absorption*

The sources listed in Table 1 together with those for which no OH absorption could be detected (Table 3) constitute a homogeneous list of the more intense continuum sources in the galactic longitude range 265°–352°. In the absence of complete galactic maps at 18 cm we have used both the Parkes 2700 MHz galactic survey and the Parkes 1410 MHz galactic survey to estimate values of T_s and T_g at 18 cm wavelength for the continuum sources searched with null results. For 74% of such sources we are able to place upper limits to τ of 0·10 or lower (see Column 4 of Table 3).

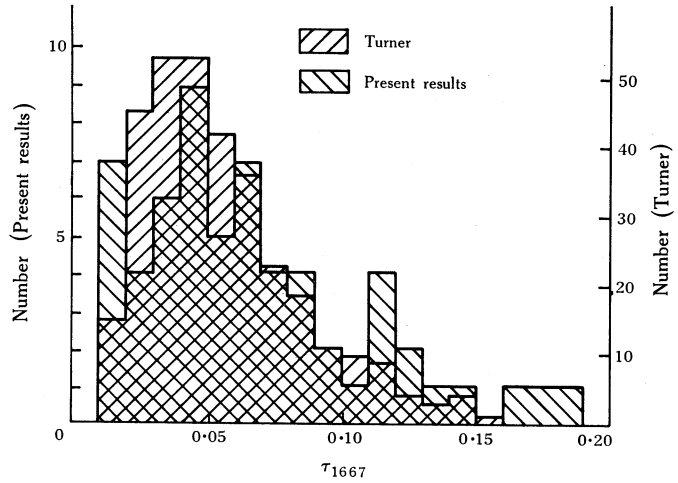

Fig. 34. Distribution of optical depth τ_{1667} in the 1667 MHz OH transition obtained from the present observations (60 features) and the observations of Turner (1972; 334 features).

Turner (1972) has discussed the statistical properties of a large number of OH absorption features observed by him. His conclusions may be compared with similar analyses of the present data, but we first note several differences between our data and that of Turner. Our coverage in galactic longitude is largely complementary to his. Our individual estimates of optical depth should be better because of our smaller beam size and our more precise measurements of continuum temperatures. However, the larger number of sources observed by Turner may result in more statistical significance for some of his conclusions. Turner's estimates for T(source) are merely values taken from maps at 11 and 21 cm as independent determinations erring from the 18 cm value in opposite directions. He comments that using $T_{(11)}$ for the continuum temperature will, for optically thin thermal sources, overestimate τ by between 1 and 2·6 according as the source is of small diameter or fills his 18′ arc beam (at 18 cm). His further statement, that when $T_{(21)}$ is used τ will be low by a factor between 1 and 1·36, appears to be in error (these values would apply if the 21 and 18 cm observations were made with the same-sized antenna); the factor actually lies between 4·6 and 1·4. Consequently τ derived from $T_{(21)}$, rather than being a better estimate than τ derived from $T_{(11)}$, tends to be a gross underestimate.

Distribution of Values of Optical Depth

The distribution of optical depths derived from our results is shown in Fig. 34, where we have also reproduced Turner's (1972) distribution (derived from $T_{(11)}$),

as given in his Fig. 8, normalized to the same area. The agreement is quite good, our median value of optical depth being 0·06 and Turner's 0·05. This good agreement would be expected if most of the continuum sources are of quite small diameter and optically thin. In contrast, Turner's distribution (his Fig. 8) derived from $T_{(21)}$ shows values of τ which are much lower, as expected from our earlier comments. Turner's comparison with the $\tau(H_2CO)$ distribution requires modification if his '11 cm' distribution of τ(OH) is much more nearly correct than his '21 cm' distribution of τ(OH). Rather than a general similarity of the H_2CO and OH distributions for τ, the optical depths encountered in H_2CO are significantly smaller than in OH.

Optical Depth as Function of Galactic Longitude

Turner (1972) concluded from his results over the galactic longitude range 337° through 360° to 75° that values of τ decrease significantly as we pass in longitude from $l < 35°$ to $l > 35°$. Since the longitude $l = 325°$ (symmetrical to $l = 35°$ about the galactic centre) lies near the middle of our data span, it is interesting to see whether a similar effect is evident here. We find that the median value of τ for clouds further from the galactic centre than $l = 325°$ is the same as that for the clouds nearer the centre. In fact, a larger proportion of clouds (6/19 compared with 6/41) with high values of τ ($>0·1$) are located further from the centre than $l = 325°$. The number of OH clouds detected is higher within 35° of the centre but this mainly reflects the presence there of a greater number of continuum sources intense enough to allow absorption measurements to be made. There is nevertheless a real increase in the density of OH within a few degrees of the galactic centre (Robinson and McGee 1970; McGee 1970).

References

Caswell, J. L. (1972). *Aust. J. Phys.* **25**, 443.
Caswell, J. L., Robinson, B. J., and Dickel, H. R. (1971). *Astrophys. Lett.* **9**, 61.
Davies, R. D., Masheder, M. R. W., and Booth, R. S. (1972). *Nature Phys. Sci.* **237**, 21.
Downes, D. (1970). *Astrophys. Lett.* **5**, 53.
Goss, W. M., Manchester, R. N., and Robinson, B. J. (1970). *Aust. J. Phys.* **23**, 559.
Hill, E. R. (1968). *Aust. J. Phys.* **21**, 735.
Johnston, K. J., Robinson, B. J., Caswell, J. L., and Batchelor, R. A. (1972). *Astrophys. Lett.* **10**, 93.
McGee, R. X. (1970). *Aust. J. Phys.* **23**, 541.
Manchester, R. N., Robinson, B. J., and Goss, W. M. (1970). *Aust. J. Phys.* **23**, 751.
Robinson, B. J., Caswell, J. L., and Goss, W. M. (1971). *Astrophys. Lett.* **9**, 5.
Robinson, B. J., Caswell, J. L., and Goss, W. M. (1974). *Aust. J. Phys.* **27**, 575.
Robinson, B. J., Goss, W. M., and Manchester, R. N. (1970). *Aust. J. Phys.* **23**, 363.
Robinson, B. J., and McGee, R. X. (1970). *Aust. J. Phys.* **23**, 405.
Schmidt, M. (1965). *In* 'Galactic Structure' (Eds. A. Blaauw and M. Schmidt), p. 513 (Univ. Chicago Press).
Shaver, P. A., and Goss, W. M. (1970). *Aust. J. Phys. astrophys. Suppl.* No. 14, 133.
Turner, B. E. (1970). *Astrophys. Lett.* **6**, 99.
Turner, B. E. (1972). *Astrophys. J.* **171**, 503.
Westerlund, B. E. (1969). *Astr. J.* **74**, 882.
Wilson, T. L., Mezger, P. G., Gardner, F. F., and Milne, D. K. (1970). *Astr. Astrophys.* **6**, 364.
Winnberg, A., Goss, W. M., Hoglund, B., and Johannson, L. E. B. (1973). *Astrophys. Lett.* **13**, 125.

Manuscript received 25 February 1974